

The intrinsic intensity modulation of PSR B1937+21 at 1410 MHz

Fredrick A. Jenet ¹, Janusz Gil²

ABSTRACT

The single-pulse properties of the millisecond radio pulsar PSR B1937+21 are studied in the 1410 MHz radio band. Aside from occasional “giant pulses” occurring in restricted regions of pulse phase, the emission appears to be remarkably stable, showing no pulse-to-pulse fluctuations other than those induced by propagation through the interstellar medium. This type of behavior has not been seen in any other pulsar although it was seen in previous 430 MHz observations of this source.

The stability of PSR B1937+21 can be understood in the context of the sparking gap model of radio pulsar emission. Given the emission properties of this source at 430 MHz, this model predicts that the emission at all higher frequencies will be just as stable. Since the stability depends on the outflow velocity of the emitting plasma, an upper bound may be placed on its Lorentz factor.

Subject headings: pulsars:general, pulsars:individual (PSR B1937+21)

1. Introduction

This letter reports on observations of the radio pulsar PSR B1937+21 taken with a center frequency of 1410 MHz at the 305m Arecibo radio telescope in Puerto Rico. Previous observations of this source at 430 MHz revealed a behavior that was completely different from other known sources (Jenet et al. 2001). At 430 MHz this source exhibits almost no detectable pulse-to-pulse fluctuations. Occasional bursts of radio radiation, or “giant pulses”, are observed but they are restricted to small regions in pulse phase (Kinkhabwala & Thorsett 2000; Cognard et al. 1996). The observations presented here show that this remarkable pulse-to-pulse stability of the non-giant pulse emission also occurs at 1410 MHz. Edwards & Stappers (2003) attempted to measure the modulation properties of PSR B1937+21 at 1300 MHz with the Westerbork synthesis radio telescope. Unfortunately, the signal-to-noise ratio in their observations was not high enough to measure the pulse-to-pulse properties.

¹California Institute of Technology, Jet Propulsion Laboratory
4800 Oak Grove Drive, Pasadena, CA 91109

²Institute of Astronomy, University of Zibeline Góra
Lubuska 2, 65-265, Zibeline Góra, Poland

Observations of bright pulsars have shown that the shapes and intensities of individual pulses are unique, although they average together to form a stable mean profile. The characteristic widths of individual pulses, typically referred to as sub-pulses, are usually smaller than the average profile width. This typical behavior has not been detected in the pulses from PSR B1937+21. Instead, this source appears to be highly stable in the sense that each pulse is identical to the next.

It will be shown that the stability of this source at both frequencies can be understood within the context of the sparking gap model of pulsar emission originally proposed by Ruderman & Sutherland (1975) and later reworked in more detail by Gil & Sendyk (2000, hereafter GS00). In this model, the stability is a result of a large number of emission regions, or “sparks”, occurring on the polar cap. The GS00 model predicts that if the emission is stable at a given frequency, then it will be stable at all higher frequencies. Since this stability will also depend on the velocity of the emitting plasma, an upper bound may be placed on its Lorentz factor.

The sparking-gap model of Ruderman & Sutherland (1975) and its revised form (GS00) have received much attention in recent years. They have been used to interpret the sub-pulse properties of slow pulsar conal emission (Edwards, Stappers, & van Leeuwen 2003; Rankin & Ramachandran 2003; van Leeuwen, Stappers, Ramachandran, & Rankin 2003; Asekar & Deshpande 2001; Deshpande & Rankin 2001) and of millisecond pulsars core emission (Edwards & Stappers 2003). These models have also been used in pulsar population studies (Arzoumanian, Chernoff, & Cordes 2002; Fan, Cheng, & Manchester 2001). Given their widespread use, it is important to develop observational tests which can determine the validity of these models. Since the GS00 model predicts that the radio emission from PSR B1937+21 should be stable at all frequencies higher than 430 MHz, high frequency observations of this source will test the current form of the GS00 model.

The next section describes the 1410 MHz observations performed at the Arecibo radio observatory. It also describes the techniques used to measure the intrinsic fluctuation properties of this source. Section 3 discusses the sparking gap model in more detail with emphasis on the frequency dependence of the modulation index. This letter is summarized in section 4.

2. Observations and Analysis

The data were taken at the 305 m Arecibo radio telescope using the 1400 MHz Gregorian dome receiver. The observation lasted two hours and approximately 4.5 million pulses were obtained. The exact center frequency used was 1410 MHz. Both circular polarizations were two-bit complex sampled at a rate of 10 MHz (100 ns) and recorded to tape using the Caltech baseband recorder (Jenet et al. 1998). Further processing of the data were performed at the Caltech Center for Advanced Computation and Research (CACR) using a 256 processor Hewlett-Packard Exemplar. The two-bit complex samples were unpacked and assigned optimum values in order to minimize signal distortion (Jenet & Anderson 1998). The dual polarization voltage data was adjusted using an empirically derived cross-talk matrix (Stineberg 1982). The effect of the Earth’s motion around

the Sun was removed by resampling the complex voltage data at a rate necessary to transform the data into the barycentric frame. This rate was calculated using the software package TEMPO³. The effects of interstellar dispersion were removed by coherently dedispersing the data (Jenet et al. 1998; Hankins & Rickett 1975) at a dispersion measure of 71.0249 pc cm³ (Jenet et al. 2001).

As with the 430 MHz observations, the single pulses from PSR B1937+21 at 1410 MHz are not bright enough to use conventional single pulse analysis techniques. Hence, the low intensity analysis methods used by Edwards & Stappers (2003) and Jenet et al. (2001) are used here. Typically, a pulsar exhibits pulse-to-pulse shape variability and intensity fluctuations. Three statistical techniques are used to determine if these phenomena are occurring in this source. First, the phase resolved modulation index is calculated in order to determine if any pulse-to-pulse amplitude fluctuations are present. Second, the average intensity fluctuation spectrum (Backer 1973) is calculated to determine the time scale of the modulation. Third, the average autocorrelation function (ACF) and the ACF of the average profile are calculated and compared to each other in order to determine if there are any pulse-to-pulse shape variations occurring. Pulse-to-pulse fluctuations may be intrinsic to the source or due to propagation through the ISM. The magnitude of the modulation index, the time scale of the modulation, and the existence of any pulse shape variations can be used to discriminate between intrinsic and ISM induced pulse-to-pulse variations.

The average pulse profile, $\langle I_s(\phi) \rangle$, normalized by its peak value is shown in figure 1. $I_s(\phi)$ is the signal intensity at pulse phase ϕ and the angle brackets, $\langle \rangle$, represent averaging over the ensemble of 4.5 million single pulses. The average profile consists of two components separated by about 520 milli-periods (mP). Note that only a small temporal region of length 425 μ s (273 mP) is shown around each component with a time resolution of .42 μ s. The giant pulses occur between 35 and 40 mP near the primary component and between 560 and 565 mP in the secondary component. The autocorrelation function of the average profile, $C_{\langle I_s \rangle}(\Delta\phi)$, is calculated for each component separately and compared to the average autocorrelation function, $\langle C_{I_s}(\Delta\phi) \rangle$, of each component. These correlation functions are defined as:

$$C_{\langle I_s \rangle}(\Delta\phi) = \frac{1}{\phi_1 - \phi_0} \int_{\phi_0}^{\phi_1} \langle I_s(\phi) \rangle \langle I_s(\phi + \Delta\phi) \rangle d\phi \quad (1)$$

$$\langle C_{I_s} \rangle(\Delta\phi) = \frac{1}{\phi_1 - \phi_0} \langle \int_{\phi_0}^{\phi_1} I_s(\phi) I_s(\phi + \Delta\phi) d\phi \rangle, \quad (2)$$

where ϕ_0 and ϕ_1 are the starting and ending pulse phases of the given emission component, respectively, and $\Delta\phi$ is the phase lag. Note that cyclic boundary conditions are assumed when evaluating the above expressions for the case when $\phi + \Delta\phi$ lies outside the interval $[\phi_0, \phi_1]$. If the individual pulses have identical shapes from pulse-to-pulse, then these two autocorrelation function will have identical shapes. Figure 2 shows both autocorrelation functions plotted together for each component. When calculating the average ACF, $\langle C_{I_s} \rangle$, the high resolution ACF was rebinned to a time

³<http://pulsar.princeton.edu/tempo>

resolution of $3.2 \mu\text{s}$ (2.05 mP) in order to increase the signal-to-noise ratio. All the of ACFs were normalized by their value at $\Delta\phi = 2.05$ mP. This corresponds to the second phase-lag bin of the rebined average ACF and was chosen to avoid the noise spike occurring in the first bin of the rebined average ACF. The solid line represents $C_{\langle I_s \rangle}(\Delta\phi)$ while the filled circles represent $\langle C_{I_s}(\Delta\phi) \rangle$. Each polarization was analyzed separately and the resulting ACFs were averaged together. The error bars were calculated using the number of points averaged together within each bin and the root-mean-square (RMS) of the data within each bin. The error bars represent the 95% confidence range. Note that even though the giant pulses are included in the ACF analysis, they will have little effect since they are very narrow and they occur infrequently.

The phase resolved modulation index is defined as

$$m(\phi) = \frac{\sqrt{\langle I_s(\phi)^2 \rangle - \langle I_s(\phi) \rangle^2}}{\langle I_s(\phi) \rangle}. \quad (3)$$

$m(\phi)$ is a measure of the pulse-to-pulse variation in intensity. Again, both polarization were analyzed separately and the resulting modulation indices were averaged together. In order to increase the signal-to-noise ratio, both $\langle I_s(\phi) \rangle$ and $\langle I_s(\phi)^2 \rangle$ were rebined to a time resolution of $3.3 \mu\text{s}$ (2.1 mP) before calculating $m(\phi)$. The error bars were calculated using the number of points averaged within each bin and the RMS values of $\langle I_s(\phi) \rangle$ and $\langle I_s(\phi)^2 \rangle$ within each bin. The error bars represent the 95% confidence range. If the amplitude of each pulse is constant and the only remaining fluctuations are due to a Gaussian statistical process, then $m(\phi)$ will be equal to 1^4 . Figure 3 plots $m(\phi)$ for both components. Only the phase region where a significant measurement could be made is shown. The modulation index is consistent with being constant across each component as expected if all pulses have the same shape. The average value of the modulation index is 1.37 ± 0.06 and 1.54 ± 0.2 for the main and secondary components, respectively.

Since pulse-to-pulse modulation is detected, it is necessary to determine if it is intrinsic to the pulsar or a result of propagation through the ISM. The expected modulation index due to the ISM alone is given by (Jenet et al. 2001):

$$m = \sqrt{1 + \frac{2}{N}}, \quad (4)$$

where N is the number of scintills in the band. N may be estimated by (Cordes et al. 1990):

$$N = 1 + \eta \frac{B}{\delta\nu}, \quad (5)$$

where B is the observing bandwidth, $\delta\nu$ is the decorrelation bandwidth and η is a packing fraction which lies between 0.1 and 0.2. Using a decorrelation bandwidth of 1.1 MHz at 1410 (Cordes 1986), m is expected to be within 1.38 and 1.48. The two dashed lines in Figure 3 represent these two values. The time scale of the fluctuations were determined by calculating the average

⁴Note that this definition of m is slightly different from the typical definition which averages down the noise before calculating m . In that case, $m = 0$ if no pulse-to-pulse fluctuations were present.

intensity fluctuation spectrum for both pulse components. Each spectrum is consistent with zero power down to a frequency of 0.02 s^{-1} . At this point, the spectrum starts to rise. This type of spectrum is indicative of the short time scale fluctuations induced by the ISM. The characteristic time scale as determined by that frequency where the power falls to half its maximum value is given by 125 s, consistent with that measured by Cordes (1986). Since the magnitude and time scale of the observed fluctuations are consistent with that expected for the ISM, it is concluded that these fluctuations are primarily due to ISM propagation and not due to intrinsic pulse-to-pulse fluctuations.

3. Intensity modulation and the sparking gap model

These results can be understood in the context of the GS00 model. In this model, a region of low charged particle density forms just above the surface of the polar cap. This “vacuum gap” is postulated to contain a number of localized plasma discharges or “sparks”. The plasma generated in each spark moves upwards following the local magnetic field. At some point, processes within the spark associated plasma generate the observed radiation with higher frequencies being emitted at lower altitudes (Melikidze, Gil & Pataraya 2000; Gil, Lyubarski & Melikidze 2003). The minimum distance between two adjacent sparks on the pulsar’s surface is approximately given by the height of the vacuum gap, h (see GS00 for details). Assuming that the polar cap is populated as densely as possible by these sparks, the total number of sparks on the cap is estimated by a^2 where a is given by

$$a = \frac{r_p}{h}, \quad (6)$$

$r_p = 10^4 R_6^{1.5} P^{-0.5}$ cm is the radius of the polar cap, R_6 is the neutron star radius in units of 10^6 cm, and P is the pulsar period in seconds. a is called the complexity parameter since it was shown by GS00 that a is correlated with the profile morphology described by Rankin (1983). Conal single profiles have the lowest values of a , followed by conal doubles and multiples and then by triple and core singles. Since a is proportional to the number of sparks that would emit into the observers line of site, the pulse-to-pulse modulation is expected to be anticorrelated with a . Possible evidence for this correlation is discussed in (Jenet & Gil 2003). PSR B1937+21 has the highest complexity parameter of all pulsars whose single pulse properties are known. Hence, its stability is a result of the large number of sparks occurring on its polar cap.

A large number of sparks on the surface is not quite enough to guarantee that the individual pulses will be stable. The emission from each spark-associated plasma column must overlap each other in order to average out the fluctuations. Since the spark plasma is moving out along the magnetic field at relativistic speeds, the angular width of the radiation pattern, Θ_r , will be given by

$$\Theta_r = \frac{1}{\gamma}, \quad (7)$$

with $\gamma = 1/\sqrt{1 - (v/c)^2}$, v is the velocity of the spark associated plasma in the radio emission

Fig. 1.— Average Pulse Profile of PSR B1937+21

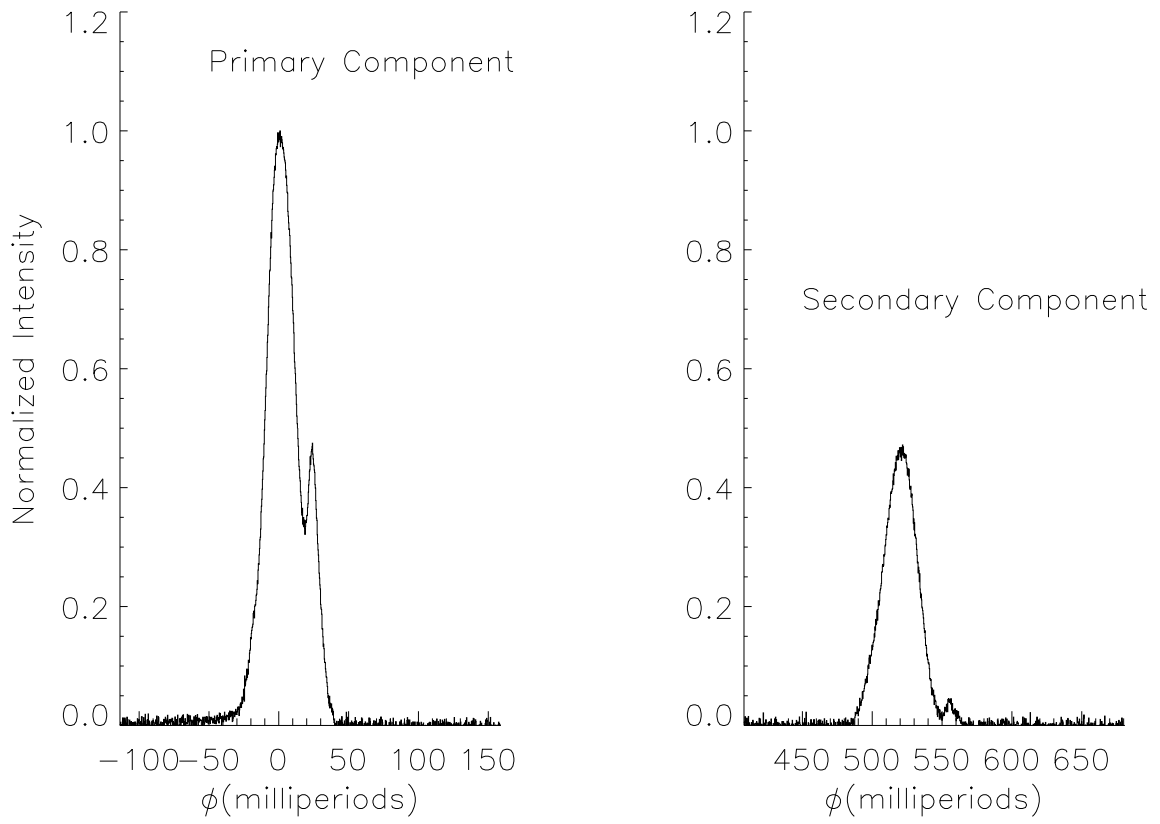


Fig. 2.— Autocorrelation functions of the primary and secondary components.

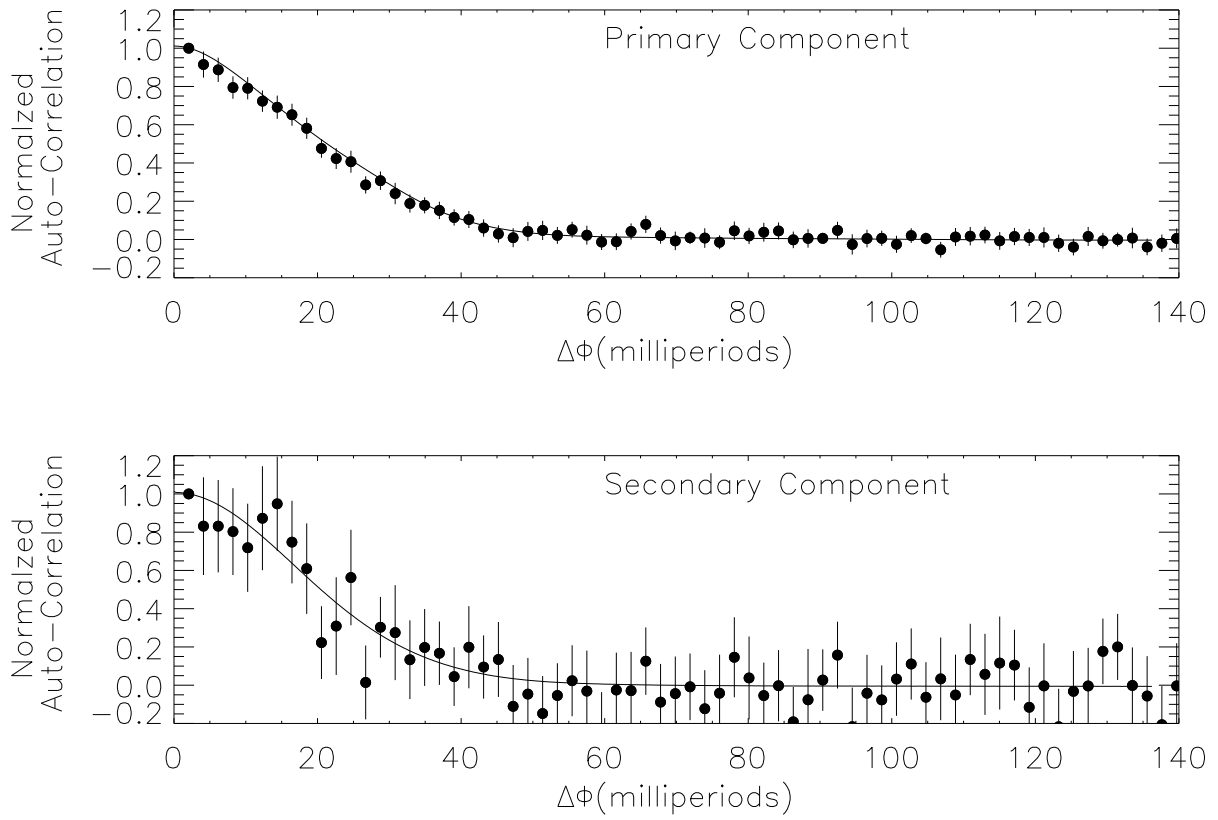
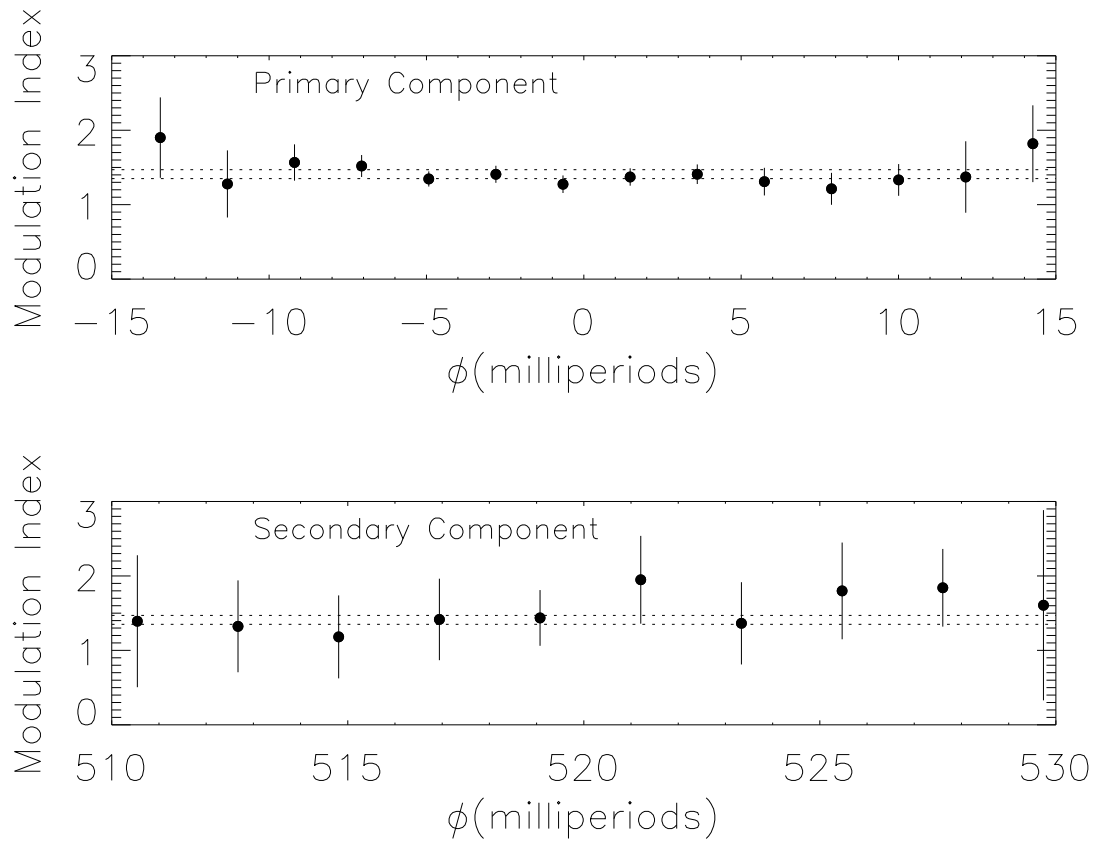


Fig. 3.— The phase resolved modulation indices of the primary and secondary components.



region, and c is the speed of light. As the spark plasma moves up along the magnetic field lines, its radiation will be beamed in a direction tangent to the local magnetic field line. Hence, the radiation from two sparks that originate near each other on the polar cap will be emitted into different directions. For a dipolar field, it turns out that the angle, $\Delta\theta$, between the radiation beams from two adjacent sparks will be given by

$$\Delta\theta = \frac{0.015}{R_6} \frac{\Delta d}{r_p} r_6^{\frac{1}{2}} P^{-\frac{1}{2}}, \quad (8)$$

where Δd is the distance between adjacent sparks on the polar cap (see GS00 for details), r_6 is the emission altitude normalized by the neutron star radius $R = R_6 10^6$ cm. In order for the emission from adjacent sparks to overlap, the following condition must be met

$$\Delta\theta < \Theta_r. \quad (9)$$

When the above equation is satisfied, the emission from adjacent sparks will overlap and the corresponding radio emission will show very little pulse-to-pulse intensity fluctuations provided that a is large. From Equations 6, 7, and 8 one can rewrite equation 9 as

$$\gamma < \frac{aR_6}{0.015} \left(\frac{P}{r_6} \right)^{\frac{1}{2}}, \quad (10)$$

where Δd was taken to be equal to h . If the emission from a given altitude satisfies the above condition, then emission from lower altitudes will also satisfy this condition. Hence, if emission from a given altitude is observed to be stable, then emission from all lower altitudes will also be stable. Observations of other pulsars point to the existence of a “radius-to-frequency” mapping which states that higher frequencies are emitted at lower altitudes (e.g. Kijak & Gil 2003). Assuming that this holds for PSR B1937+21, the pulses emitted at 1410 MHz are expected to be at least as stable as those emitted at 430 MHz.

Since the observations are in agreement with the spark gap model described above, one can go one step further and use Equation 10 to place an upper bound, γ_{max} , on the Lorentz factor of the emitting plasma. The following form of the radius-to-frequency map will be used (Kijak & Gil 2003):

$$r_6(\nu_{GHz}) = 40\nu_{GHz}^{-0.26} \dot{P}_{-15}^{0.07} P^{0.3}, \quad (11)$$

where ν_{GHz} is the observing frequency in GHz and \dot{P}_{-15} is the pulsar period derivative in 10^{-15} s/s. For PSR B1937+21, $r_6(0.43) = 5.5$ and $a = 23$. Hence, Equation 10 yields $\gamma_{max} = 26R_6$. This estimate assumes the standard vacuum gap model described by RS75. For the case of the near threshold vacuum gap (NTVG) model (Gil & Melikidze 2002), a can be up to 3.5 times higher than that estimated by equation 6 since a will depend on the actual value of the surface magnetic field line radius of curvature. In this case, $\gamma_{max} = 91R_6$.

4. Summary and Discussion

Radio observations of the millisecond pulsar PSR B1937+21 were taken at a center frequency of 1410 MHz. Statistical techniques were used to determine if this source exhibits any of the standard single pulse phenomenology that has been seen in other radio pulsars. Remarkably, none of the usual phenomena were detected. The data are consistent with each pulse having the same shape and intensity. Previously, Jenet et al. (2001) showed that this source exhibits the same single pulse stability at 430 MHz. This stability is currently unique to this source. Hence, PSR B1937+21 maybe the prototype for a new class of radio pulsars. On the other hand, the sparking gap model provides a unified framework that can explain this source's behaviour as an extreme case of the normal pulsar emission process. In the context of the GS00 model, the stability is a result of a large number of sparks occurring on the polar cap together with a low Lorentz factor of the emitting plasma. Since the 430 MHz observations show no pulse-to-pulse fluctuations, the GS00 model predicts that all higher frequencies will be just as stable provided higher frequencies are emitted at lower altitudes. This result is independent of the exact physical model used to describe the vacuum gap. Future observations of this source at several frequencies above 430 MHz will further test the GS00 model. If fluctuations are seen, then the current form of the sparking gap model is incorrect. Observations of this source at frequencies below 430 MHz will enable a better measurement of the Lorentz factor. If pulse-to-pulse fluctuations are seen at lower frequencies, a lower bound may be placed on γ for a given model of the vacuum gap.

Part of this research was performed at the Jet Propulsion Laboratory, California Institute of Technology, under contract with the National Aeronautics and Space Administration. GJ acknowledges the support of the Polish State Committee for scientific research under grant 2 P03D 008 19.

REFERENCES

- Arzoumanian, Z., Chernoff, D. F., & Cordes, J. M. 2002, *ApJ*, 568, 289
- Asgekar, A. & Deshpande, A. A. 2001, *MNRAS*, 326, 1249
- Backer, D. C. 1973, *ApJ*, 182, 245
- Cognard, I., Shrauner, J. A., Taylor, J. H., & Thorsett, S.E. 1996, *ApJ*,457,L81
- Cordes, J. M. 1986, *ApJ*, 331, 183
- Cordes, J. M., Wolszczan, A., Dewey, R. J., Blaskiewicz, M., & Stinebring, D. R. 1990, *ApJ*, 349, 245
- Deshpande, A. A. & Rankin, J. M. 2001, *MNRAS*, 322, 438

- Edwards, R. T. & Stappers, B. W. 2003, *A&A*, 407, 273
- Edwards, R. T., Stappers, B. W., & van Leeuwen, A. G. J. 2003, *A&A*, 402, 321
- Fan, G. L., Cheng, K. S., & Manchester, R. N. 2001, *ApJ*, 557, 297
- Gil, J., & Sendyk, M. 2000, *ApJ*, 541, 351 (GS00)
- Gil, J., Lyubarski, Y., & Melikidze, G. 2003, *ApJ*, in press (astro-ph/0301621)
- Gil, J. & Melikidze, G.I. 2002, *ApJ*, 577, 909
- Hankins, T. H. & Rickett, B. J. 1975, *Methods in Computational Physics. Volume 14 - Radio astronomy*, 14, 55
- Jenet, F. A. & Anderson, S. B. 1998, *PASP*, 110, 1467
- Jenet, F., Anderson, S., Kaspi, V., Prince, T., & Unwin, S. 1998, *ApJ*, 498, 365
- Jenet, F., Anderson, S. B., & Prince, T.A. 2001, *ApJ*, 546, 394
- Jenet, F. A. & Gil, J. 2003, *ApJ*, 596, L215
- Kijak, J., & Gil, J. 2003, *A&A*, 397, 969
- Kinkhabwala, A. & Thorsett, S. E. 2000, *ApJ*, 535, 365
- Melikidze, G.I., Gil, J. & Pataraya, A.D., 2000, *ApJ*, 544, 1081
- Rankin J. M., 1983, *ApJ*, 274, 333
- Rankin, J. M. & Ramachandran, R. 2003, *ApJ*, 590, 411
- Ruderman, M. A., & Sutherland, P. G. 1975, *ApJ*, 196,51 (RS75)
- Stineberg, D. R. 1982, Ph.D. Thesis,
- van Leeuwen, A. G. J., Stappers, B. W., Ramachandran, R., & Rankin, J. M. 2003, *A&A*, 399, 223